

# Numerical simulation of reinforced concrete slabs under missile impact

Duc-Kien Thai<sup>a</sup> and Seung-Eock Kim<sup>\*</sup>

*Department of Civil and Environmental Engineering, Sejong University,  
98 Kunja-dong, Kwangjin-ku, Seoul, 143-747, South Korea*

*(Received September 21, 2013, Revised May 17, 2014, Accepted July 13, 2014)*

**Abstract.** This paper presents a numerical analysis of reinforced concrete slabs under missile impact loading. The specimen used for the numerical simulation was tested by the Technical Research Center of Finland. LS-DYNA, commercial available software, is used to analyze the model. The structural components of the reinforced concrete slab, missile, and their contacts are fully modeled. Included in the analysis is material nonlinearity considering damage and failure. The results of analysis are then verified with other research results. Parametric studies with different longitudinal rebar ratios, shear bar ratios, and concrete strengths are conducted to investigate their influences on the punching behavior of slabs under the impact of a missile. Finally, efficient designs are recommended.

**Keywords:** missile impact; reinforced concrete slabs; LS-DYNA; dynamic analysis; punching behavior

---

## 1. Introduction

The ability of reinforced concrete structures to protect against severe impact has become increasingly important to ensure public safety. For a better understanding of the behavior of reinforced concrete structures subjected to impact loading, several experimental studies have been carried out. Recent researches have focused on predicting the punching resistance of structures by measuring the local effects on the structures, such as the penetration depth, scabbing area, and perforation.

A series of studies on reinforced concrete slabs with the dimensions of 2.1 m×2.1 m×0.25 m under missile impact loading have carried out. A medium-scaled impact test was designed by Lastunen *et al.* (2007). Several experiments on slabs with and without shear bars were performed by Saarenheimo *et al.* (2009), Vepsä *et al.* (2011) to investigate the punching resistance of the reinforced concrete slabs by missiles.

Although the experimental approach can provide reliable results of slab behavior, it is expensive and time consuming. As finite element analysis has been a useful alternative, a number of numerical studies were carried out by Saarenheimo *et al.* (2009), Tuomala *et al.* (2010), Martin *et al.* (2012). The objective of their numerical simulation is to capture the response and

---

<sup>\*</sup>Corresponding author, Professor, E-mail: [sekim@sejong.ac.kr](mailto:sekim@sejong.ac.kr)

<sup>a</sup>Ph.D. Student

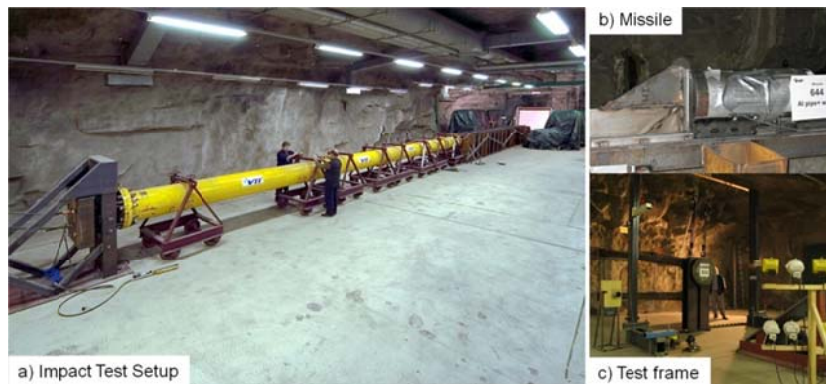


Fig. 1 RC slab impact test facility (Saarenheimo *et al.* 2009)

behavior of the reinforced concrete slab subjected to high-rate impact loading. The finite element analysis is an appropriate and efficient solution for large sized structures that cannot be accommodated through the experimental method.

In all of the experimental as well as the numerical studies mentioned above, the longitudinal rebar ratio was 0.7%, the shear bar ratios were from 0.62% to 1.4%, and the compressive strengths of concrete were from 50MPa to 70MPa. In practical design as recommended in Eurocode-2 (2004), the common range of longitudinal rebar ratio is 0.13% to 4%, the shear bar ratio is higher than 0.12%, and the compressive strength is 40MPa to 90MPa. Because of the variety of the reinforcement ratios and concrete strengths, a wide range of these variables should be studied. Moreover, researches on the optimal design regarding longitudinal rebar and shear bar ratio have not been carried out. In this paper, parametric studies with different longitudinal rebar ratios, shear bar ratios, and concrete strengths were conducted to investigate their influence on the punching behavior of slabs under missile impact. Efficient designs were recommended.

## 2. Description of the models

### 2.1 Geometry

The specimens tested by Vepsä *et al.* (2011) were used in this study. The impact test facility, created by the Technical Research Center of Finland (Saarenheimo *et al.* 2009) is shown in Fig. 1. A schematic representation of the reinforced concrete slab with a shear bar is shown in Fig. 2. The dimensions of the two-way slab is 2.1 m×2.1 m×0.25 m. The slab includes longitudinal rebars of 10 mm diameter at 90 mm spacing in each direction. The shear bars are placed at 90 mm spacing at the intersection of every longitudinal rebar. The edges of the slab are encased by steel plates of 10 mm thickness. The slab is clamped to a steel frame through the rollers of 35 mm diameter as shown in Fig. 3. The steel frame is installed to a massive wall.

A schematic representation of the missile is shown in Fig. 4. The missile consists of a steel pipe of 168 mm outside diameter and 10mm thickness. In order to have enough mass and rigidity, the missile is filled with lightweight concrete. The missile has approximately a total mass of 47 kg and a length of 640 mm.

Two types of models were used in this analysis. The first model, named AM-1, was tested by

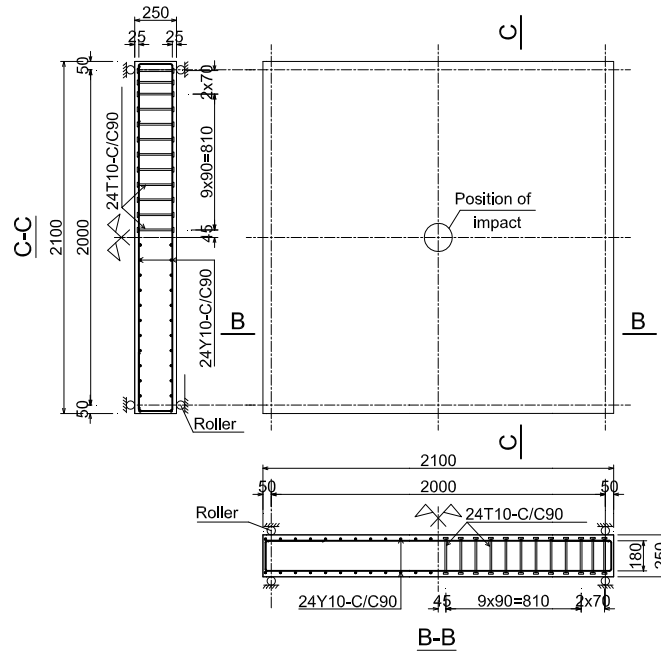


Fig. 2 Geometry of slab

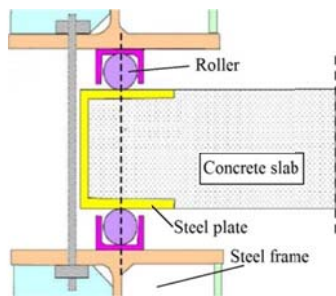


Fig. 3 Support system

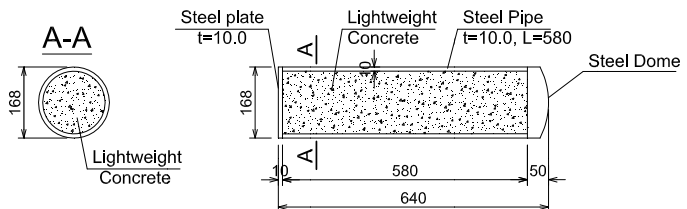


Fig. 4 Geometry of missile

Vepsä *et al.* (2011). In this model, only the longitudinal rebar was used. The second model, named AM-2, was geometrically similar to AM-1. In this model, shear bars were added to the slab. The model AM-1 was used for the verification of analysis results and for the parametric study with different longitudinal rebar ratios and concrete strengths. Model AM-2 was used for the parametric study with different shear bar ratios and for optimal design with combinations of longitudinal rebar ratio, shear bar ratio, and concrete strength.

## 2.2 Material properties

The material properties tested by Vepsä *et al.* (2011) were used in this study. The unconfined compressive strength of the concrete slab was 64.7 MPa. The yield strength of the steel rebar was 540 MPa. The yield strength of steel cover plate, frame, and roller was 500 MPa. The failure strain of steel rebar was 18.67%. The yield strength of the steel missile was 758 MPa. The compressive

Table 1 Material properties

Material	Modulus of elastic $E$ (GPa)	Poisson Ratio $\nu$	Density $\rho$ (Kg/m <sup>3</sup> )	UCS (MPa)	UTS (MPa)	Failure strain (%)	Fract. Energy (N/m)
Concrete for slab	27.535	0.17	2400	64.7	3.34	-	95
Lightweight concrete	10.6	0.17	1158	3	1	-	95
Steel for rebar	200	0.3	7800	540	540	18.67	-
Steel for missile	200	0.3	7800	758	758	-	-
Steel for cover plate	200	0.3	7800	500	500	-	-

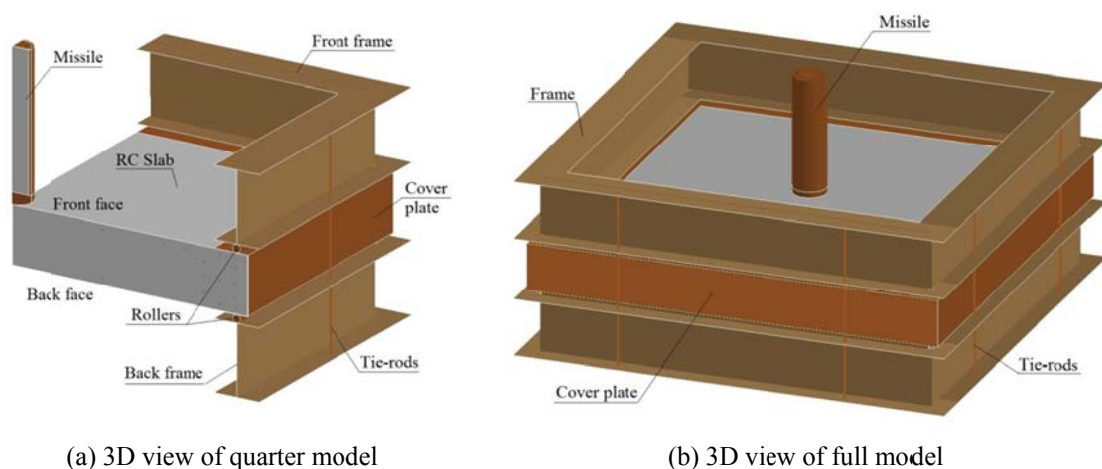


Fig. 5 Finite element model of RC slab with frame and missile

strength of the concrete missile filler was 3 MPa. Table 1 shows the material properties of the concrete, rebar, and other metal parts in detail.

### 3. Finite element modelling

#### 3.1 General

The finite element code, LS-DYNA (version 971s R5.1.1) was used for analysis. Due to the symmetry of geometry and impact loading, only a quarter of the slab and missile was modeled as shown in Fig. 5(a). The full model in Fig. 5(b) was generated using the quarter model for easily understanding. The concrete slab, longitudinal rebar, shear bars, cover plates, rollers, frame, supporting-pipes, and missile were modeled in separate parts and assembled to make the full model. The appropriate constrains and contacts were applied between them.

#### 3.2 Element type and mesh

The components of the reinforced concrete slab, missile, and frame were modeled as shown in Fig. 6. The concrete slab in Fig. 6(a) was modeled with the 8-node solid element. The longitudinal

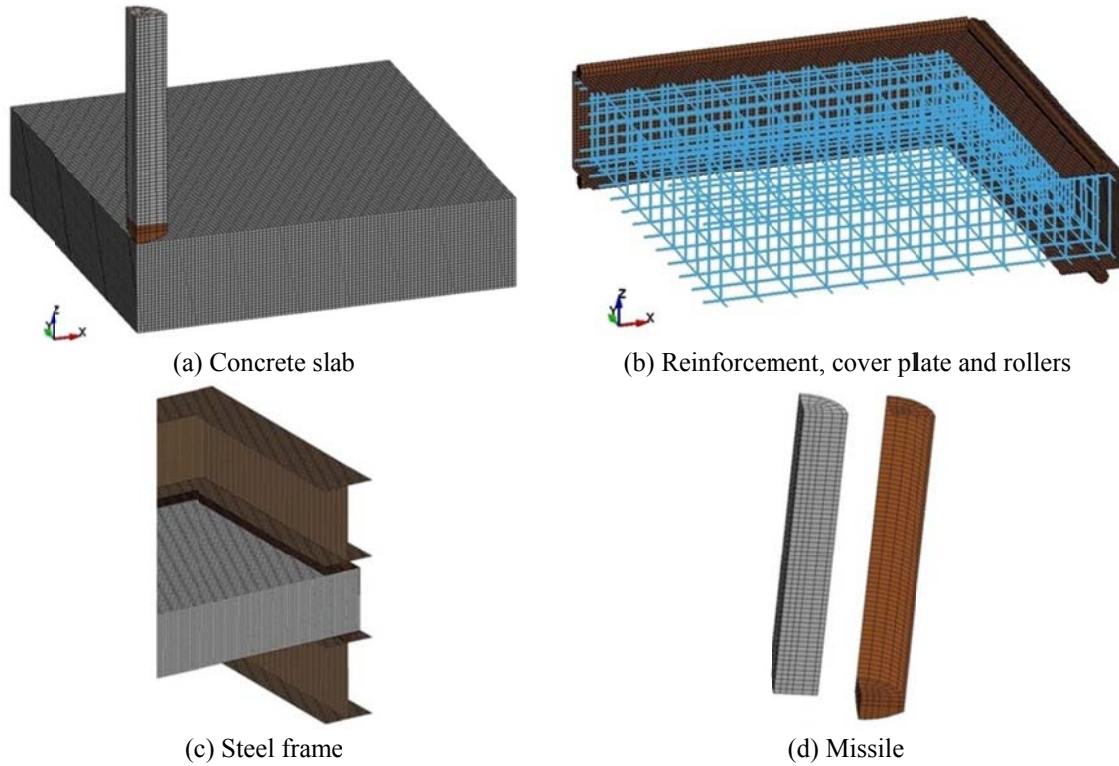


Fig. 6 Finite element type and mesh

Table 2 Total element numbers of a quarter of model AM-2

Components	Beam elements	Shell elements	Solid elements
Slab	-	-	330,750
Rebars	3,352	-	-
Missile	-	381	1,674
Frame	-	28,000	-
Cover-plate	-	12,150	-
Roller	-	-	7,920
Tie-rods	6	-	-
Back-pipe	1	-	-
Total	3,359	40,531	340,344

and shear bars were modeled using the beam element as shown in Fig. 6(b). The cover plates and frame were modeled with the Belytschko-Tsay shell element as shown in Fig. 6(c). The rollers were modeled by using the solid element. The missile-head and the concrete filler were modeled by using the solid element, whereas the missile cover plate was modeled with the shell element as shown in Fig. 6(d).

The bond between the concrete filler and the missile cover plate as well as the missile head was also considered by using shared nodes. The general mesh size was 10 mm. The total number of the elements of the components of the quarter model is shown in Table 2.

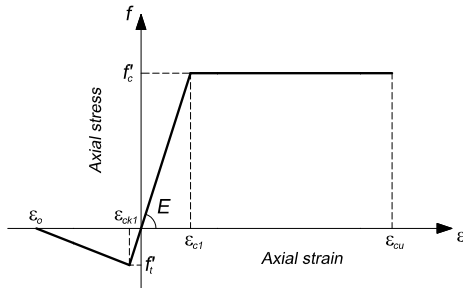


Fig. 7 Bi-linear concrete model

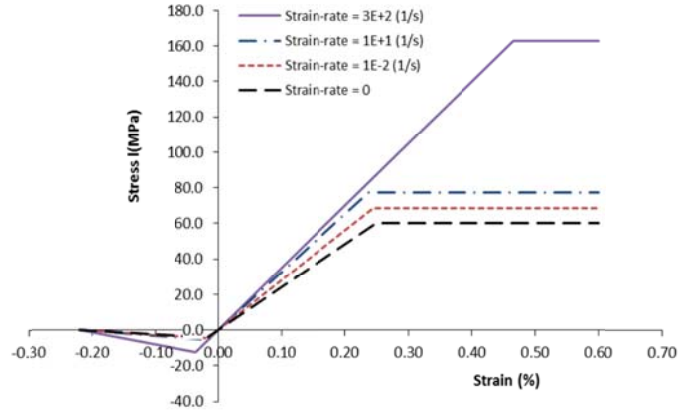


Fig. 8 Stress-strain curves of concrete with various strain-rates

### 3.3 Material model

#### 3.3.1 Concrete

The Winfrith material model (MAT#084) considering strain-rate in LS-DYNA (2007) was used for the slab and lightweight concrete material. The bi-linear concrete model using an equivalent uniaxial stress-strain curve shown in Fig. 7 was used. The elastic-plastic curve with the ultimate strain ( $\varepsilon_{cu}$ ) at failure was assumed for the concrete compressive model. The linear tension softening behavior with the axial strain ( $\varepsilon_{ck1}$ ) at failure was assumed for concrete tension model. The tensile fracture strain ( $\varepsilon_0$ ) was determined as a function of the fracture energy of the concrete.

The Winfrith concrete model does not consider the erosion effect. The erosion option for damage and failure was considered by using the option \*MAT\_ADD\_EROSION. This option has total 14 different erosion criteria. According to the sensitivity studies conducted by Sagals *et al.* (2011), the principal strain was shown to be the most sensitive erosion criterion. The erosion criteria of  $\pm 7.5\%$  were used in this study since it was determined by comparison with experiments.

The strain-rate effect is considered automatically in the Winfrith concrete model. Fig. 8 shows the stress-strain curves with respect to various strain-rates as an example regarding the effect of the strain-rate. Concrete with the static compressive strength of 64.7 MPa was used. The concrete strengths were calculated by multiplying the original values with that of strain-rate enhancement factors. The tensile ( $E_T$ ) and compressive ( $E_C$ ) factors were calculated using the following equations (Schwer 2010)

- With the low strain-rate, when  $\dot{\varepsilon} < 30s^{-1}$

$$E_T = \left( \frac{\dot{\varepsilon}}{\dot{\varepsilon}_{0T}} \right)^{1.016\delta} \quad \text{and} \quad E_C = \left( \frac{\dot{\varepsilon}}{\dot{\varepsilon}_{0C}} \right)^{1.026\alpha} \quad (1)$$

- With the high strain-rate, when  $\dot{\varepsilon} > 30s^{-1}$

$$E_T = \eta \dot{\varepsilon}^{1/3} \quad \text{and} \quad E_C = \gamma \dot{\varepsilon}^{1/3} \quad (2)$$

where  $\delta = \frac{1}{10 + 0.5f_{cu}}$ ;  $\alpha = \frac{1}{5 + 0.75f_{cu}}$ ;  $\log_{10} \eta = 6.933\delta - 0.492$ ;  
 $\log_{10} \gamma = 6.156\alpha - 0.49$ ;  $\dot{\epsilon}_{0T} = 30 \times 10^{-6} s^{-1}$ ; and  $\dot{\epsilon}_{0C} = 3 \times 10^{-6} s^{-1}$

Here,  $f_{cu}$  is the concrete cube strength (unit in MPa).

The Young's modulus rate enhancement was calculated using the following equation

$$E_E = 0.5 \left[ \left( \frac{\dot{\epsilon}}{\dot{\epsilon}_{0T}} \right)^{0.016} + \left( \frac{\dot{\epsilon}}{\dot{\epsilon}_{0C}} \right)^{0.026} \right] \quad (3)$$

### 3.3.2 Rebar and structural steel

The elastic plastic with kinematic hardening material model (MAT#003) in LS-DYNA (2007) was used for the rebar and structural steel as shown in Fig. 9. In this study, kinematic hardening was considered by setting the parameter  $\beta=0$ .

The yield strength of the rebar and structural steel is highly strain rate dependent. This increases when the strain-rate increases. This dynamic yield strength of steel was taken into consideration by the Cowper-Symonds formula for uniaxial tension or compression (Marais *et al.* 2004)

$$\frac{\sigma_d}{\sigma_s} = 1 + \left( \frac{\dot{\epsilon}}{C} \right)^{\frac{1}{P}} \quad (4)$$

where  $\sigma_d$  is the dynamic yield strength,  $\sigma_s$  is the static yield strength,  $\dot{\epsilon}$  is the strain-rate, and  $C$  and  $P$  are constants of the Cowper-Symonds relation. For the rebar and structural steel, the constants  $C=40.4 s^{-1}$  and  $P=5$  proposed by Jones (2012) were used. Fig. 10 shows the stress-strain curves with respect to the various strain-rates of the steel with yield strength of 540 MPa.

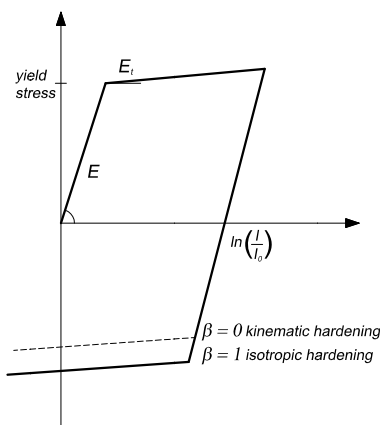


Fig. 9 Elastic-plastic behavior with kinematic/isotropic hardening

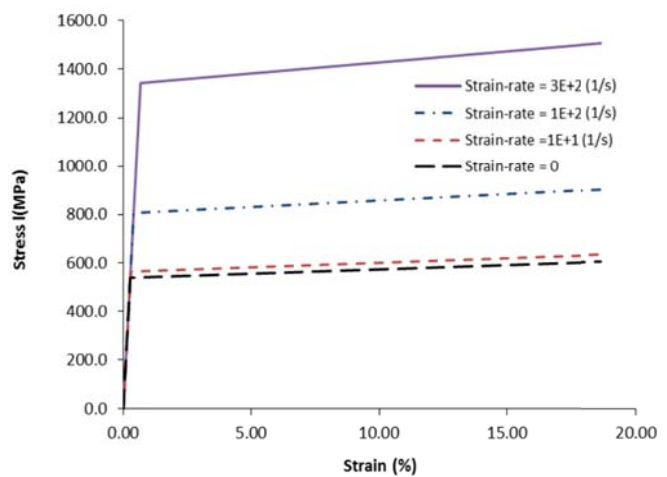


Fig. 10 Stress-strain curves of steel with various strain-rates



Fig. 11 Test specimen (Saarenheimo *et al.* 2009)

### 3.4 Contact and boundary condition

The component models were assembled by appropriate constraints and contacts. The rebar was embedded in the concrete using the option `*CONSTRAINED_LARGRANGE_IN_SOLID`. The contact was applied between the reinforced concrete slab (through the cover plates) and the rollers using the option `*AUTOMATIC_SURFACE_TO_SURFACE`. The rollers were also attached to the steel frame by sharing their nodes. The supporting-pipes were attached to the frame through their common nodes. The fixed boundary conditions were applied to the end-nodes of the supporting-pipes, and symmetric boundary conditions were applied at the reference nodes of the mid-span sections of the model. The perfect bond between missile cover plate, missile head, and concrete filler were considered by sharing their nodes.

The option `*AUTOMATIC_SURFACE_TO_SURFACE` was used for the missile-slab contact, whereas `*AUTOMATIC_NODES_TO_SURFACE` was used for the missile-rebar contact. For the missile-slab contact, the segment set of the missile was defined as the slave part, whereas the segment set of the concrete slab was defined as the master part. For the missile-rebar contact, the node set of the rebar was defined as the slave, while the segment set of the missile was defined as the master part.

## 4. Verification of finite element model

An initial velocity of 136 m/s was applied to the missile nodal set using the option `*INITIAL_VELOCITY`. In order to reduce the analysis time, the missile head was located directly on the face of the slab. The analysis time of 20 ms was selected in order to observe complete missile perforation. The time interval of 1E-4 seconds was applied for getting continuous behavior. Hourglass control with the stiffness form of Flanagan-Belytschko integration (IHQ=4) was selected.

The Winfrith concrete model can calculate crack width. The crack width of the concrete element was calculated using the option `*DATABASE_BINARY_D3CRACK`. In this analysis, the fracture energy (FE) of 95N/m recommended in *fib* MC2010 (2013) was used.

A recent experiment conducted by Vepsä *et al.* (2011) was used to verify the proposed FE model. The experiment specimen clamped by the test frame is shown in Fig. 11.

Table 3 Comparison with test results conducted by Vepsä *et al.* (2011)

Method	Initial velocity (m/s)	Failure mode	Residual velocity (m/s)	Scabbing Area (m <sup>2</sup> )
Test	136	Perforation	45	1.00
FEM	136	Perforation	47	1.25
Difference	0	-	4.4%	25.0%

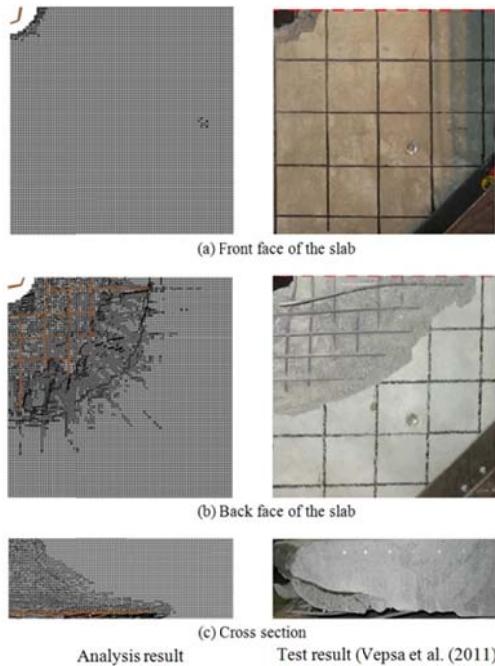


Fig. 12 Comparison of Scabbing areas

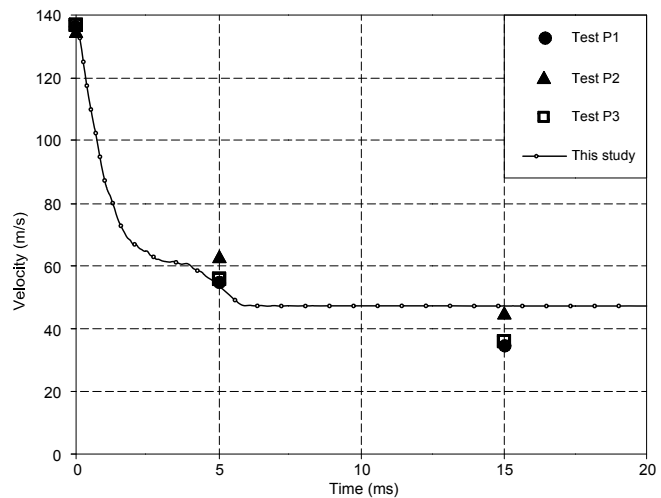


Fig. 13 Missile velocities during the first 20 ms after impact

The residual velocity, scabbing area, and failure mode obtained from the test and finite element analysis are compared in Table 3. The residual velocity was taken at 15 ms after the beginning of impact. The scabbing area was obtained using the erosion option with the failure strain criteria of  $\pm 7.5\%$ . An acceptable agreement was achieved between experimental and numerical results. The specimen was perforated in both the test and FE modeling. The scabbing area agreed well between the experiment and numerical analysis as shown in Fig. 12. Fig. 13 compares the missile velocity (m/s) after impact between the analysis and test results provided by Vepsä *et al.* (2011). The curve closely matched the results of the test P2. As a result, the developed finite element model reliably predicted the failure mode and damage of the reinforced concrete slab under impact loading.

### 5. Parametric study

Three parametric studies were conducted to investigate the influence of the longitudinal rebar, shear bar, and concrete strength on the punching response of RC slabs. Different missile initial velocities of 70 m/s, 136 m/s, and 190 m/s were applied in order to consider its influence on the response of the RC slabs. Specimens similar to those of Vepsä *et al.* (2011) were used.

Table 4 Longitudinal rebar ratios for specimens in the first parameter study

Specimen	Diameter of rebar (mm)	Area (m <sup>2</sup> )	Ratio (%)
LR-1	8	0.0000502	0.45
LR-2	10	0.0000785	0.70
LR-3	12	0.0001130	1.00
LR-4	14	0.0001539	1.37
LR-5	16	0.0002010	1.79
LR-6	18	0.0002543	2.26
LR-7	20	0.0003140	2.79
LR-8	22	0.0003799	3.38

Table 5 Shear bar ratios for specimens in the second parameter study

Specimen	Diameter of rebar (mm)	Area (m <sup>2</sup> )	Ratio (%)
SR-1	8	0.0000502	0.62
SR-2	10	0.0000785	0.97
SR-3	12	0.0001130	1.40
SR-4	14	0.0001539	1.90
SR-5	16	0.0002010	2.48

Table 6 Concrete compressive strengths for specimens in the third parameter study

Specimen	Compressive strength $f'_c$ (MPa)	Tensile strength $f'_t$ (MPa)	Elastic modulus $E$ (MPa)
CCS-1	40	2.50	22857
CCS-2	50	2.90	28571
CCS-3	60	3.10	31579
CCS-4	70	3.20	35000
CCS-5	80	3.40	36364
CCS-6	90	3.50	39130

Table 7 Concrete tensile strengths for specimens in the third parameter study

Specimen	Compressive strength $f'_c$ (MPa)	Approximate equation	Tensile strength $f'_t$ (MPa)
CTS-1	60	$3\sqrt{f'_c}$	1.93
CTS-2		$4\sqrt{f'_c}$	2.57
CTS-3		$5\sqrt{f'_c}$	3.22
CTS-4		$6\sqrt{f'_c}$	3.86
CTS-5		$7\sqrt{f'_c}$	4.50
CTS-6		$8\sqrt{f'_c}$	5.15

The eight impact test specimens, as listed in Table 4, were investigated in the first parametric study. The specimens had different longitudinal rebar ratios of 0.45% to 3.38% as each direction. The material properties of slab, rebar, frame, and missile are listed in Table 1. Table 5 shows a list

of five test specimens with the different shear bar ratios of 0.62% to 2.48%. These test specimens were investigated in the second parametric study. The third parametric study investigated six specimens with different concrete compressive strengths of 40 MPa to 90 MPa as listed in Table 6. In the Table 7, the typical tensile strength ranges of concrete were calculated by  $f'_t=3(f'_c)^{1/2}$  to  $f'_t=8(f'_c)^{1/2}$  as presented by Nilson *et al.* (2010), where  $f'_c$  is expressed in psi units. The LR-2 reinforcement of 10 mm diameter with 90 mm spacing was used in the slabs of Tables 5, 6, and 7.

The analysis results of the distance travelled (the term “distance travelled” used in this study means the distance travelled by the missile head from 0 ms to 20 ms), scabbing area, and failure mode are summarized in Tables 8-11. The observed damage of the reinforced concrete slab is classified into the following five modes:

- Fully Perforated (FP) Mode: The missile passed through the slab completely.
- Partially Perforated (PP) Mode: The missile stopped at the back layer of the longitudinal rebar.

Table 8 Analysis results of parameter studies of longitudinal rebar ratios

Initial velocity of the missile	Specimen	Dis. travelled (m)	Scabbing area (m <sup>2</sup> )	Failure mode*
70 m/s	LR-1	0.138	0.000	PS
	LR-2	0.108	0.000	PS
	LR-3	0.104	0.000	PS
	LR-4	0.103	0.000	PS
	LR-5	0.094	0.000	P
	LR-6	0.093	0.000	P
	LR-7	0.088	0.000	P
	LR-8	0.086	0.000	P
136 m/s	LR-1	1.208	1.020	FP
	LR-2	1.052	1.246	FP
	LR-3	0.780	1.766	FP
	LR-4	0.420	2.834	PP
	LR-5	0.383	2.543	PP
	LR-6	0.362	2.111	PP
	LR-7	0.326	1.452	PP
	LR-8	0.312	0.916	PP
190 m/s	LR-1	2.280	0.785	FP
	LR-2	2.208	0.950	FP
	LR-3	2.131	1.246	FP
	LR-4	1.990	1.410	FP
	LR-5	1.836	1.910	FP
	LR-6	1.554	2.377	FP
	LR-7	1.140	2.716	FP
	LR-8	0.863	2.954	FP

\* FP= Fully Perforated Mode, PP = Partially Perforated Mode, PS= Partially Scabbed Mode, P= Penetration Mode.

Table 9 Analysis results of parameter studies of shear bar ratios

Initial velocity of the missile	Specimen	Dis. travelled (m)	Scabbing area (m <sup>2</sup> )	Failure mode *
70 m/s	SR-1	0.113	0.000	PS
	SR-2	0.116	0.126	FS
	SR-3	0.106	0.011	FS
	SR-4	0.102	0.126	FS
	SR-5	0.213	0.113	FS
136 m/s	SR-1	1.289	0.166	FP
	SR-2	1.306	0.152	FP
	SR-3	1.340	0.152	FP
	SR-4	1.394	0.138	FP
	SR-5	1.404	0.132	FP
190 m/s	SR-1	2.426	0.212	FP
	SR-2	2.432	0.166	FP
	SR-3	2.460	0.166	FP
	SR-4	2.423	0.181	FP
	SR-5	2.455	0.166	FP

\* FP= Fully Perforated Mode, FS= Fully Scabbed Mode, PS= Partially Scabbed Mode.

Table 10 Analysis results of parameter studies of concrete compressive strength

Initial velocity of the missile	Specimen	Dis. travelled (m)	Scabbing area (m <sup>2</sup> )	Failure mode *
70 m/s	CCS-1	0.122	0.000	PS
	CCS-2	0.123	0.000	PS
	CCS-3	0.109	0.000	PS
	CCS-4	0.107	0.000	PS
	CCS-5	0.108	0.000	PS
	CCS-6	0.105	0.000	PS
136 m/s	CCS-1	1.137	1.168	FP
	CCS-2	1.160	1.056	FP
	CCS-3	1.124	1.056	FP
	CCS-4	1.126	0.985	FP
	CCS-5	1.089	1.168	FP
	CCS-6	1.035	1.130	FP
190 m/s	CCS-1	2.319	0.817	FP
	CCS-2	2.243	0.849	FP
	CCS-3	2.172	0.849	FP
	CCS-4	2.146	0.849	FP
	CCS-5	2.127	0.882	FP
	CCS-6	2.089	1.056	FP

\* FP= Fully Perforated Mode, PS= Partially Scabbed Mode.

Table 11 Analysis results of parameter studies of concrete tensile strength

Initial velocity of the missile	Specimen	Dis. travelled (m)	Scabbing area (m <sup>2</sup> )	Failure mode*
70 m/s	CTS-1	0.179	0.000	PS
	CTS-2	0.119	0.000	PS
	CTS-3	0.112	0.000	PS
	CTS-4	0.105	0.000	PS
	CTS-5	0.096	0.000	PS
	CTS-6	0.091	0.000	PS
136 m/s	CTS-1	1.340	0.817	FP
	CTS-2	1.210	1.020	FP
	CTS-3	1.121	1.020	FP
	CTS-4	1.053	1.056	FP
	CTS-5	0.960	1.056	FP
	CTS-6	0.880	1.168	FP
190 m/s	CTS-1	2.361	0.636	FP
	CTS-2	2.271	0.694	FP
	CTS-3	2.150	0.849	FP
	CTS-4	2.102	0.916	FP
	CTS-5	2.050	1.020	FP
	CTS-6	1.993	1.020	FP

\* FP= Fully Perforated Mode, PS= Partially Scabbed Mode.

- *Fully Scabbed (FS) Mode*: The missile stuck into the slab and the shear cone failure occurred at back of the slab.

- *Partially Scabbed (PS) Mode*: The missile stuck into the slab and shear cone cracks formed at back of the slab, but scabbing mode was prevented.

- *Penetration (P) Mode*: A crater formed at the front face of the slab, but shear cone cracks except only few small cracks did not form at the back face of the slab.

### 5.1 Longitudinal rebar ratios

The behavior of model AM-1 with eight different longitudinal rebar (LR) ratios applied with different missile velocity impacts was investigated. The ratios of 0.45% to 3.38% were used by utilizing the eight different diameters of rebar elements from 8 mm to 22 mm, as listed in Table 4.

#### 5.1.1 Distance travelled

Fig. 14 shows the distance travelled corresponding to the different longitudinal rebar ratios. As the longitudinal rebar ratios increased, the distance travelled decreased. In case of the missile initial velocity of 70 m/s, the distance travelled slightly decreased from 0.138 m to 0.086 m when the longitudinal rebar ratios increased from 0.45% to 3.38%. In case of the missile initial velocity of 136 m/s, the distance travelled rapidly decreased from 1.208 m to 0.420 m when the longitudinal rebar ratios increased from 0.45% to 1.37%. However, the distance travelled decreased slightly from 0.420 m to 0.312 m when the longitudinal rebar ratios increased from

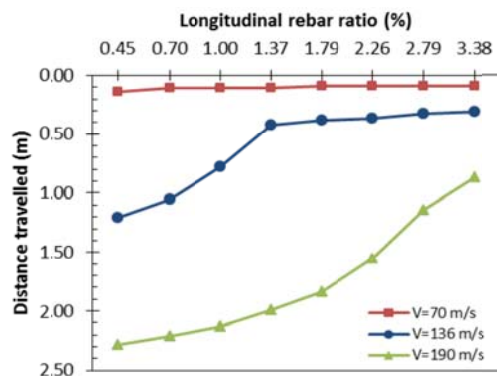


Fig. 14 Dis. travelled with respect to LR ratio

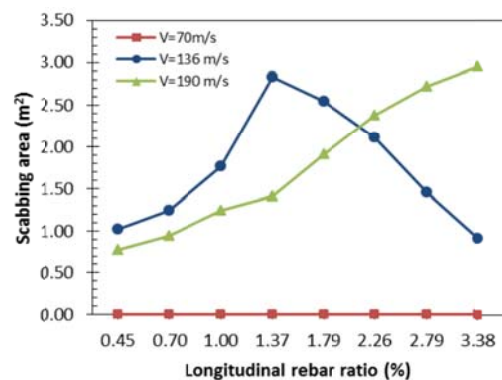


Fig. 15 Scabbing areas with respect to LR ratio

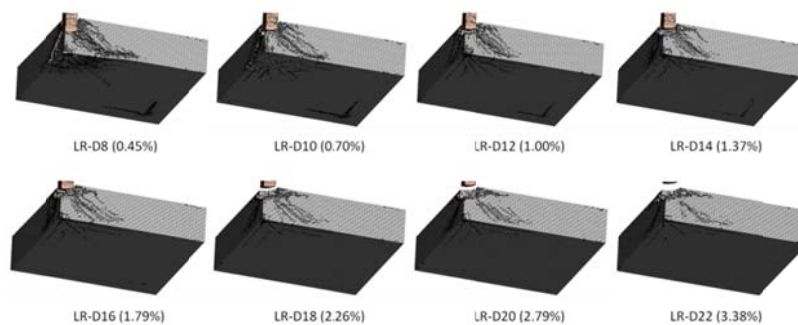


Fig. 16 Failure modes of RC slabs under impacts of missile (velocity of 70 m/s)

1.37% to 3.38%. In case of the missile initial velocity of 190 m/s, the distance travelled rapidly decreased from 2.280 m to 0.863 m when the longitudinal rebar ratios increased from 0.45% to 1.37%. It is observed that the longitudinal rebar plays an important role in resisting perforation of the reinforced concrete slab. The analysis results also showed that the slope of the curves increased as the velocity of the missile increased. This indicates that punching resistance of the slabs increased when the velocity of the missile increased due to the strain-rate effect of the material.

### 5.1.2 Scabbing area

Fig. 15 shows the relationship between the scabbing area and the longitudinal rebar ratio. Scabbing did not occur in case of the applied velocity of 70 m/s. In case of the missile initial velocity of 136 m/s, the scabbing area rapidly increased from 1.020 m<sup>2</sup> to 2.834 m<sup>2</sup> as the longitudinal rebar ratios increased from 0.45% to 1.37%. However, the scabbing area rapidly decreased from 2.834 m<sup>2</sup> to 0.916 m<sup>2</sup> when the longitudinal rebar ratios increased from 1.37% to 3.38%. In case of the missile initial velocity of 190 m/s, the scabbing area rapidly increased from 0.785 m<sup>2</sup> to 2.954 m<sup>2</sup> as the longitudinal rebar ratios increased from 0.45% to 3.38%. The longitudinal rebar ratio also significantly influences the scabbing area at the back face of the slab.

### 5.1.3 Failure mechanism

Fig. 16-21 show the failure modes and scabbing areas as per the eight different longitudinal rebar ratios at the time of 20 ms.

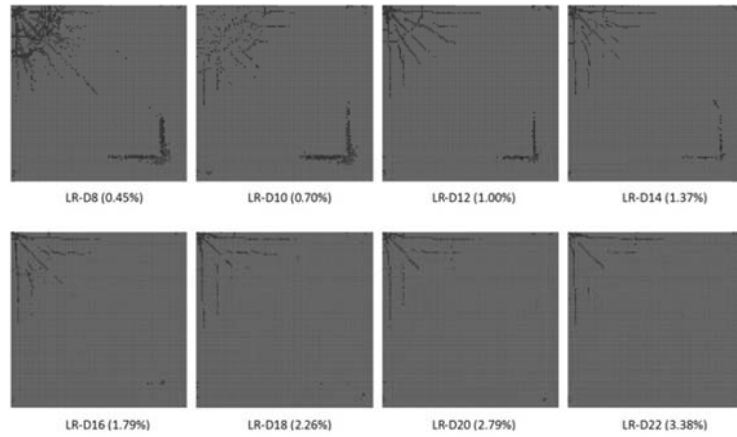


Fig. 17 Scabbing areas on the back face of the slab (velocity of 70 m/s)

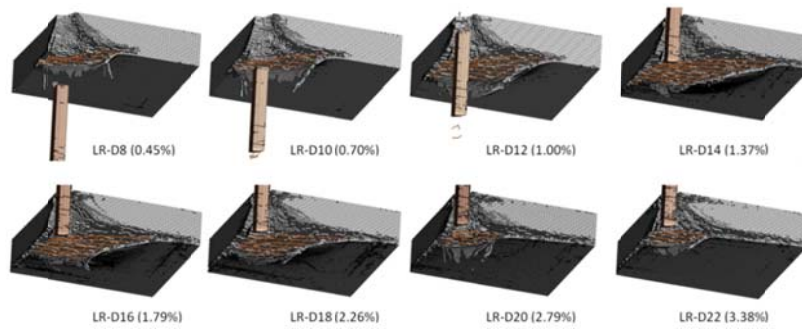


Fig. 18 Failure mode of RC slabs under impacts of missile (velocity of 136 m/s)

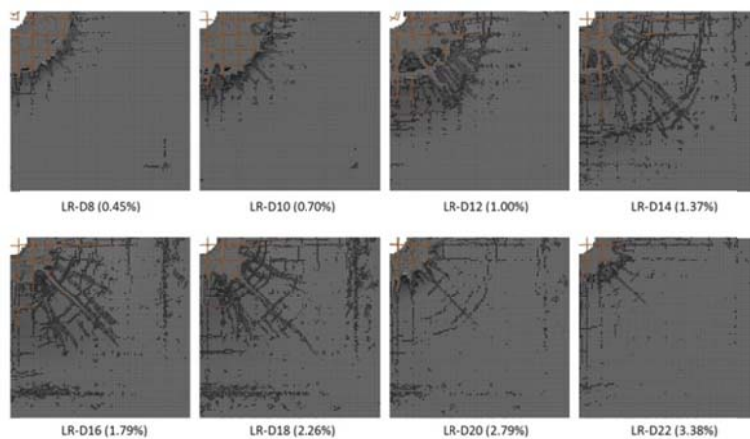


Fig. 19 Scabbing areas on the back face of the slab (velocity of 136 m/s)

In case of the missile initial velocity of 70 m/s (see Figs. 16-17), when the longitudinal rebar ratios were smaller than 1.79%, a significant fracture occurred, but scabbing was prevented due to the punching resistance of the back layers of the longitudinal rebars. When the longitudinal rebar

ratios were higher than 1.79%, shear cone cracks formed at the back face of the slab, but no significant fracture occurred. In this case, the perforation was prevented due to the punching resistance provided by the front layer of the longitudinal rebars.

In case of the missile initial velocity of 136 m/s (see Figs. 18-19), the missile passed through the reinforced concrete slab when the longitudinal rebar ratios were from 0.45% to 1.0%. However, the missile stopped at the back layer of the longitudinal rebars when the ratios were equal or higher than 1.37%. This is due to the punching resistance of the back layer of the longitudinal rebars. When the longitudinal rebar ratios increased from 0.45% to 1.37%, the displacement of the back layer rebars increased due to a corresponding increase in impact force transfer from missile to the said rebars. The displacement of the rebars caused the concrete cover layer to be separated. As a result, the scabbing area increased as longitudinal rebar ratios increased. However, when the longitudinal rebar ratio increased from 1.37% to 2.38%, the displacement of

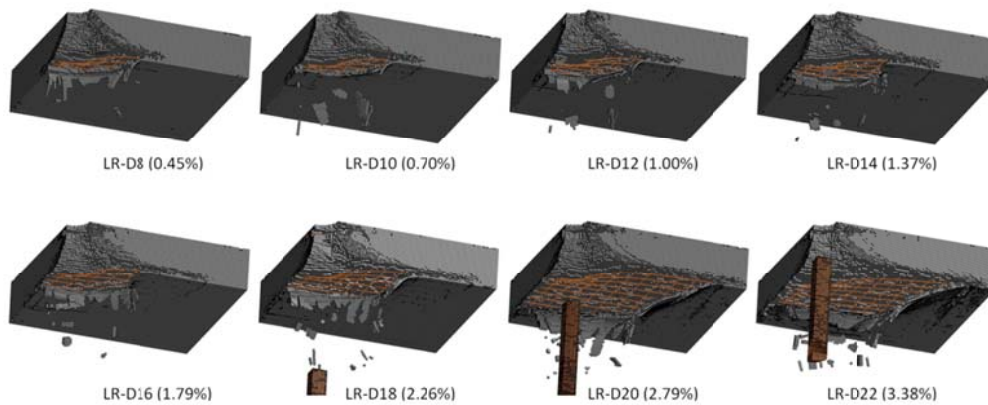


Fig. 20 Failure modes of RC slabs under impacts of missile (velocity of 190 m/s)

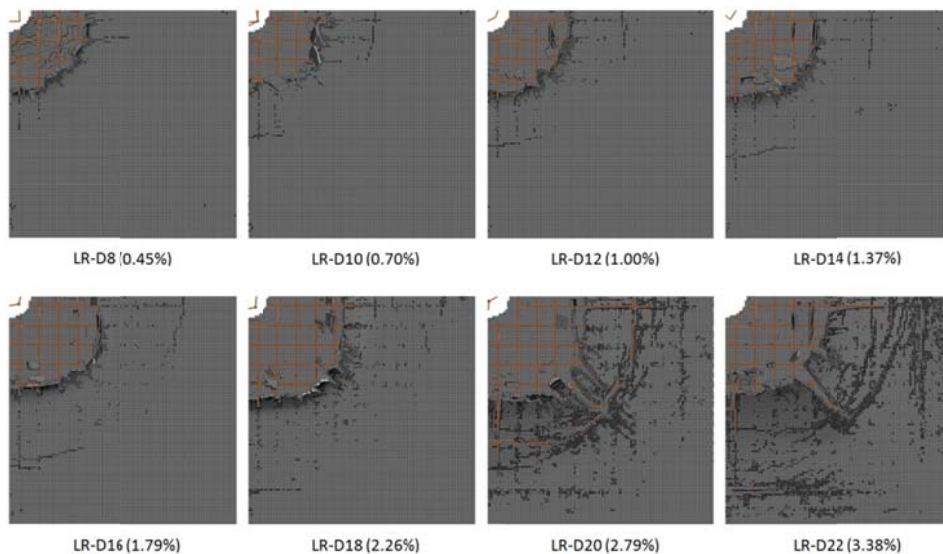


Fig. 21 Scabbing areas on the back face of the slab (velocity of 190 m/s)

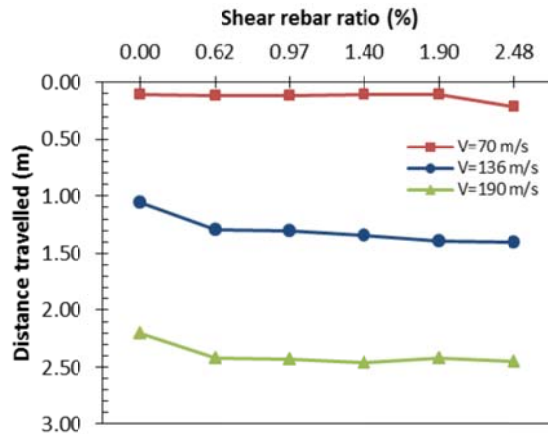


Fig. 22 Dis. travelled with respect to SR ratio

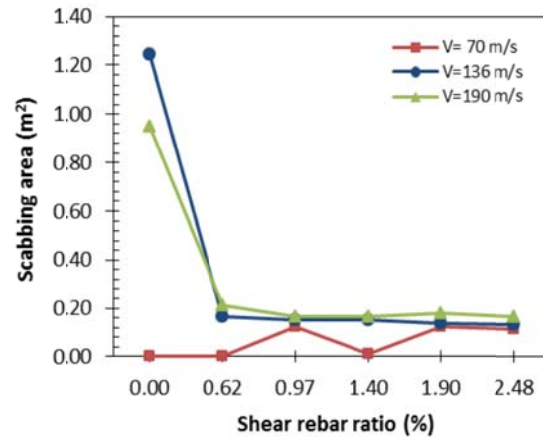


Fig. 23 Scabbing areas with respect to SR ratio

the back layer rebars decreased due to bending resistance of the rebars. These rebars prevented the increase of scabbing area of the RC slabs. As a result, the scabbing area decreased as longitudinal rebar ratios increased.

In case of the missile initial velocity of 190 m/s (see Figs. 20-21), the missile passed through the reinforced concrete slab in all cases. As the longitudinal rebar ratios increased, the scabbing area increased due to a significant displacement of the rebars as explained previously.

## 5.2 Shear bar ratios

The behavior of model AM-2 with six different shear rebar (SR) ratios was investigated. The ratios of 0.62% to 2.48% were used as listed in Table 5.

### 5.2.1 Distance travelled

Fig. 22 shows the distance travelled corresponding to the different shear bar ratios. In case of the missile initial velocity of 70 m/s, the distance travelled increased slightly from 0.108 m to 0.213 m as the shear bar ratios increased from 0% to 2.48%. In case of the missile initial velocity of 136 m/s, the distance travelled increased slightly from 1.052 m to 1.404 m as the shear bar ratios increased from 0% to 2.48%. In case of the missile initial velocity of 190 m/s, the distance travelled increased slightly from 2.208 m to 2.455 m as the shear bar ratios increased from 0% to 2.48%. It was observed that the use of shear bar did not provide any beneficial effect regarding perforation resistance.

### 5.2.2 Scabbing area

The shear bar ratio significantly influences the scabbing area on the slab's back face, as shown in Fig. 23. In case of the missile initial velocity of 70 m/s, when the shear bar ratios increased from 0% to 0.62%, the scabbing area did not occur. However, when the shear bar ratios increased from 0.62% to 2.48%, the scabbing area oscillated within the range of 0.011 m<sup>2</sup> to 0.126 m<sup>2</sup>. In case of the missile initial velocity of 136 m/s, when the shear bar ratios increased from 0% to 0.62%, the scabbing area rapidly decreased from 1.246 m<sup>2</sup> to 0.166 m<sup>2</sup>. When the shear bar ratios increased from 0.62% to 2.48%, the scabbing area slightly decreased from 0.166 m<sup>2</sup> to 0.132 m<sup>2</sup>. In case of

the missile initial velocity of 190 m/s, when the shear bar ratios increased from 0% to 0.62%, the scabbing area rapidly decreased from 0.950 m<sup>2</sup> to 0.212 m<sup>2</sup>. When the shear bar ratios increased from 0.62% to 2.48%, the scabbing area slightly decreased from 0.212 m<sup>2</sup> to 0.166 m<sup>2</sup>.

### 5.2.3 Failure mechanism

Figs. 24-29 show the failure modes and scabbing areas as per the six different shear bar ratios at the time of 20 ms.

In case of the missile initial velocity of 70 m/s (see Figs. 24-25), the case without shear bars showed an occurrence of significant fracture while scabbing was prevented. When the shear bar ratios were in the range of 0.62% to 1.4%, shear cone cracks formed at the back face of the slab but no significant fracture occurred. Shear bar ratios from 1.90% to 2.48% resulted to scabbing but no perforation of missile to RC slab.

In case of the missile initial velocity of 136 m/s (see Figs. 26-27) and 190 m/s (see Figs. 28-29), perforation occurred in all cases. The scabbing area decreased as shear bar ratios increased.

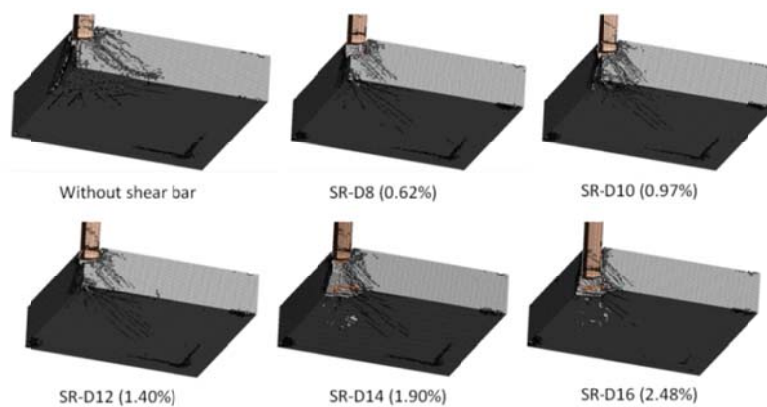


Fig. 24 Failure mode of RC slabs under impacts of missile (velocity of 70 m/s)

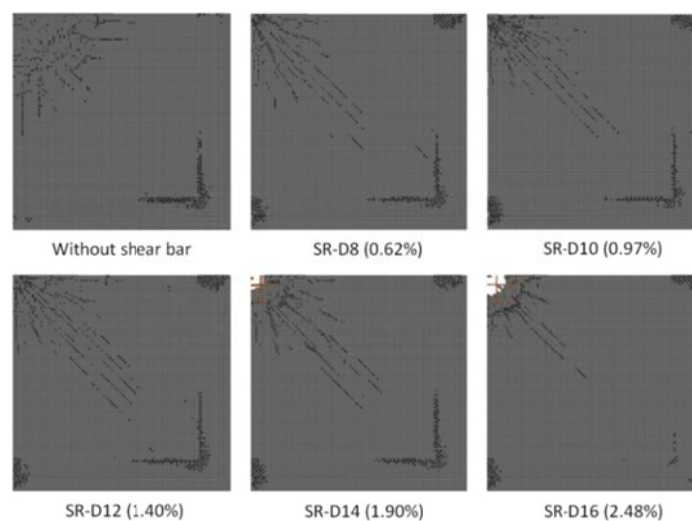


Fig. 25 Scabbing areas on the back face of the slab (velocity of 70 m/s)

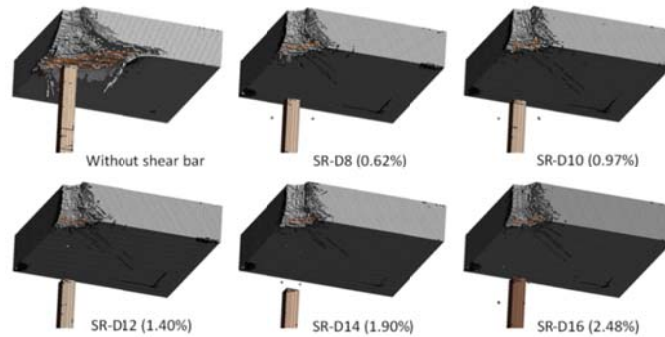


Fig. 26 Failure mode of RC slabs under impacts of missile (velocity of 136 m/s)

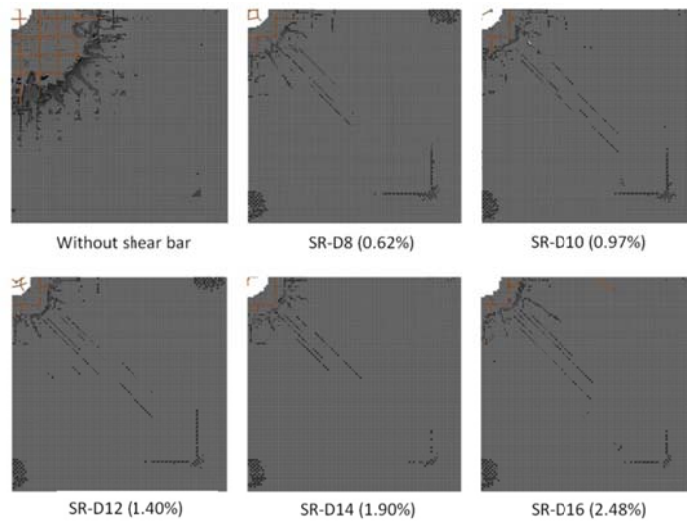


Fig. 27 Scabbing areas on the back face of the slab (velocity of 136 m/s)

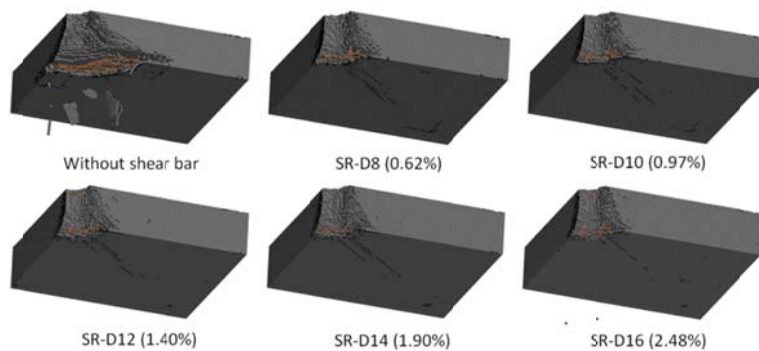


Fig. 28 Failure mode of RC slabs under impacts of missile (velocity of 190 m/s)

The effect of shear bars in the RC slab is explained as follows:

The shear bars made the concrete slab stiffer. The slab with lower shear bar ratio undergoes greater deflection. The deformation of the slab absorbs energy from the missile and dampens the

impact loading. In case the higher shear bar ratio was used, the bending stiffness of the slab became higher, and the damaging energy transferred from missile to the concrete slab eased. As the result, the distance travelled increased when the shear bar ratio increased.

The scabbing area in the concrete slab caused by the missile impact load can be divided into shear cone and scabbing zone as shown in Fig. 30. The shear cone was perforated by the shear stress generated by the perforation force of the missile. The shear bar played the role of improving the shear force, while the longitudinal rebar had a minimal effect on penetrating the shear core. As a result, the scabbing area decreased when the shear bar ratio increased. Part of the energy of the missile made the longitudinal rebar deformed significantly. The longitudinal rebar caused the concrete cover to be separated from the slab. In this analysis, both ends of the shear bar were assumed to be connected to the longitudinal rebar on both sides by sharing their nodes. As the shear bar ratio increased, the deformation of the longitudinal rebar decreased and the scabbing area was reduced.

### 5.3 Concrete strength

The behavior of the model AM-1 with six different concrete compressive strengths (CCS), and six different concrete tensile strengths (CTS) applied with different missile velocity impacts was investigated. The concrete compressive strengths of 40 MPa to 90 MPa were listed in Table 6. The concrete tensile strengths of 1.93 MPa to 5.15 MPa were calculated using different approximate equations based on its compressive strength of 60 MPa as shown in Table 7.

#### 5.3.1 Distance travelled

The analysis results showed that increasing the compressive strength of concrete did not provide any significant effect on the perforation resistance of the reinforced concrete slabs as shown in Fig. 31. In case of the missile initial velocity of 70 m/s, the distance travelled oscillated within the range of 0.105 m to 0.123 m when the concrete compressive strength increased from 40

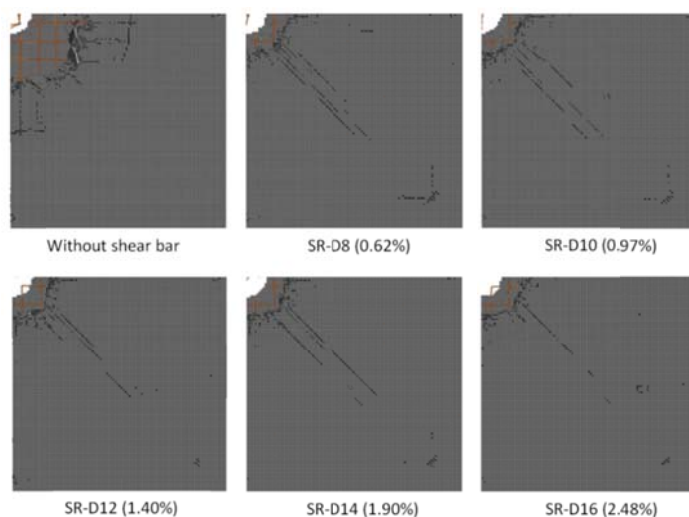
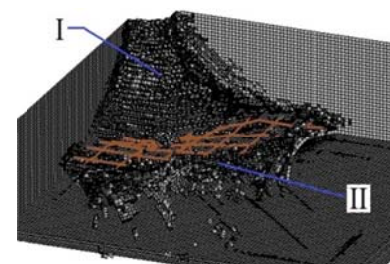


Fig. 29 Scabbing areas on the back face of the slab (velocity of 190 m/s)



(I) Shear cone, (II) Scabbing zone

Fig. 30 Scabbing areas in concrete slab

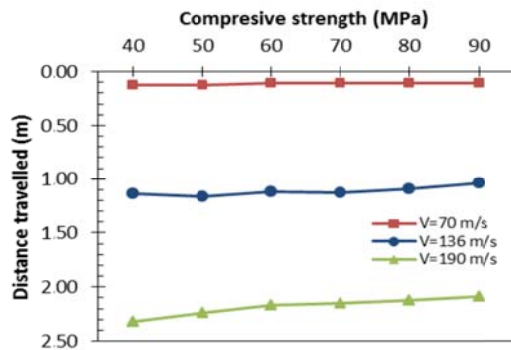


Fig. 31 Dis. travelled with respect to concrete compressive strength

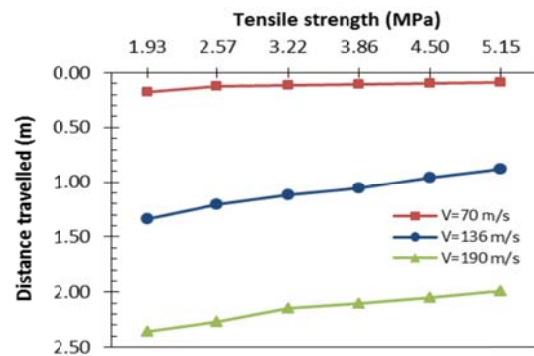


Fig. 32 Dis. travelled with respect to concrete tensile strength

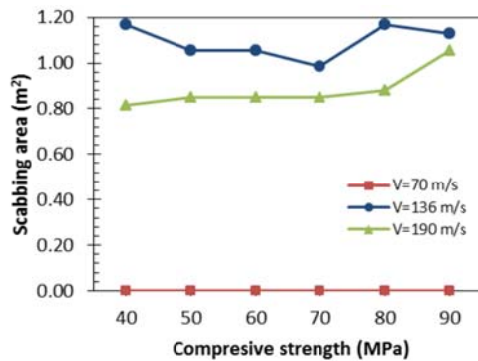


Fig. 33 Scabbing areas with respect to concrete compressive strength

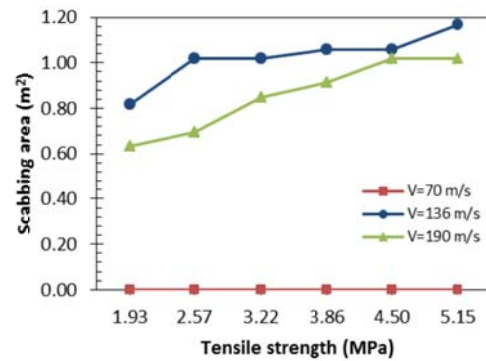


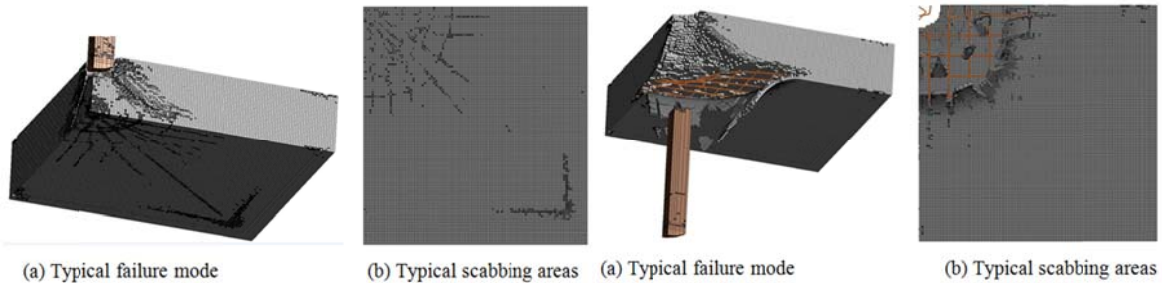
Fig. 34 Scabbing areas with respect to concrete tensile strength

MPa to 90 MPa. In case of the missile initial velocity of 136 m/s, the distance travelled slightly decreased from 1.137 m to 1.035 m when the concrete compressive strength increased from 40 MPa to 90 MPa. In case of the missile initial velocity of 190 m/s, the distance travelled slightly decreased from 2.319 m to 2.089 m when the concrete compressive strength increased from 40 MPa to 90 MPa.

The concrete tensile strength had a significant effect on the perforating resistance of the reinforced concrete slabs as shown in Fig. 32. In case of the missile initial velocity of 70 m/s, the distance travelled slightly decreased from 0.179 m to 0.091 m when the tensile strength increased from 1.93 MPa to 5.15 MPa. In case of the missile initial velocity of 136 m/s, the distance travelled rapidly decreased from 1.340 m to 0.880 m when the tensile strength increased from 1.93 MPa to 5.15 MPa. In case of the missile initial velocity of 190 m/s, the distance travelled rapidly decreased from 2.361 m to 1.993 m when the tensile strength increased from 1.93 MPa to 5.15 MPa.

### 5.3.2 Scabbing area

Fig. 33 shows the relationship between the scabbing area and the concrete compressive strength. In general, the analysis results showed that the compressive strength did not provide any significant effect on reducing the scabbing area of the reinforced concrete slabs. Scabbing area did



(a) Typical failure mode

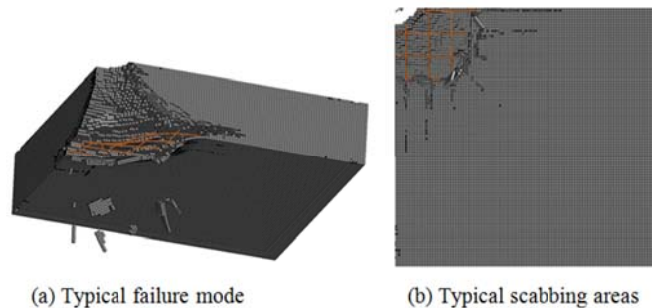
(b) Typical scabbing areas

Fig. 35 Typical failure mode and scabbing area of RC slabs (velocity of 70 m/s)

(a) Typical failure mode

(b) Typical scabbing areas

Fig. 36 Typical failure mode and scabbing area of RC slabs (velocity of 136 m/s)



(a) Typical failure mode

(b) Typical scabbing areas

Fig. 37 Typical failure mode and scabbing area of RC slabs (velocity of 190 m/s)

not occur when the missile initial velocity of 70 m/s was applied. In case of the missile initial velocity of 136 m/s, the scabbing area oscillated within the range of 0.985 m<sup>2</sup> to 1.168 m<sup>2</sup> as the compressive strength changed within the range of 40 MPa to 90 MPa. In case of the missile initial velocity of 190 m/s, the scabbing area increased from 0.817 m<sup>2</sup> to 1.056 m<sup>2</sup> as the compressive strength changed within the range of 40 MPa to 90 MPa.

The relationship between the scabbing area and the tensile strength of the concrete is shown in Fig. 34. In general, as the tensile strength increased, the scabbing area increased. Scabbing area did not occur when the missile initial velocity of 70 m/s was applied. In case of the missile initial velocity of 136 m/s, the scabbing area increased from 0.817 m<sup>2</sup> to 1.020 m<sup>2</sup> as the tensile strength increased from 1.93 MPa to 2.57 MPa. The scabbing area slightly decreased from 1.020 m<sup>2</sup> to 1.056 m<sup>2</sup> when the tensile strength increased from 2.57 MPa to 4.50 MPa, but the scabbing area increased from 1.056 m<sup>2</sup> to 1.168 m<sup>2</sup> when the tensile strength increased from 4.50 MPa to 5.15 MPa. In case of the missile initial velocity of 190 m/s, the scabbing area increased from 0.636 m<sup>2</sup> to 1.020 m<sup>2</sup> as the tensile strength increased from 1.93 MPa to 5.15 MPa.

### 5.3.3 Failure mechanism

Figs. 35-37 show the typical failure modes and scabbing areas at the time of 20 ms. In case of the missile initial velocity of 70 m/s (see Fig. 35(a)-(b)), the significant fracture occurred, but scabbing was prevented and the missile did not perforate the RC slab. In case of the missile initial velocity of 136 m/s (see Fig. 36(a)-(b)), the full perforation occurred in all cases. In case of the missile initial velocity of 190 m/s (see Fig. 37(a)-(b)), full perforation occurred in all cases and the missile passed through and away from the slab at a significant distance.

### 6. Optimal design

This section presents the optimal design of the RC slab considering resistance to the impact of a missile with initial velocity of 136 m/s. In order to determine the efficient combination of the reinforcement for optimal design, the behavior of the model AM-2 with different combinations of longitudinal rebar and shear bar were conducted. The perforation limit is the most important criterion to guarantee safety. Based on the parameter studies, the following ranges of parameters should be used for optimal design:

- (1) Longitudinal rebar ratios should be from 1.37% to 2.26%
- (2) Shear bar ratios should be from 0.62% to 1.90%

Table 12 shows the analysis results of the six design models. Fig. 38 compares the distance travelled at 20 ms. Analysis result shows that Design-3 has the smallest distance travelled, whereas Design-4 has the greatest distance travelled.

Fig. 39 compares the scabbing areas on the back face of the slabs composed of different designs. The analysis results showed that all of the designs have scabbing areas in the range of 0.152 m<sup>2</sup> to 0.229 m<sup>2</sup>. It can be observed that Design-5 has the smallest scabbing area, whereas Design-3 has the largest scabbing area.

From the above comparisons, it can be concluded that in cases where the purpose of the design is to resist perforation of the slab, Design-3 should be used. Otherwise, if the purpose of the design is to reduce the scabbing area, then Design-5 should be used.

Table 12 Analysis results of design models

Specimen	Long. rebar (LR) dia. (mm)	Shear rebar (SR) dia. (mm)	Dis. travelled (m)	Scabbing area (m <sup>2</sup> )	Failure mode *
Design -1	14	10	1.000	0.166	FP
Design -2	16	10	0.808	0.166	FP
Design -3	18	10	0.324	0.229	PP
Design -4	14	12	1.034	0.166	FP
Design -5	16	12	0.884	0.152	FP
Design -6	18	12	0.748	0.166	FP

\* FP= Fully Perforation Mode, PP = Partially Perforation Mode.

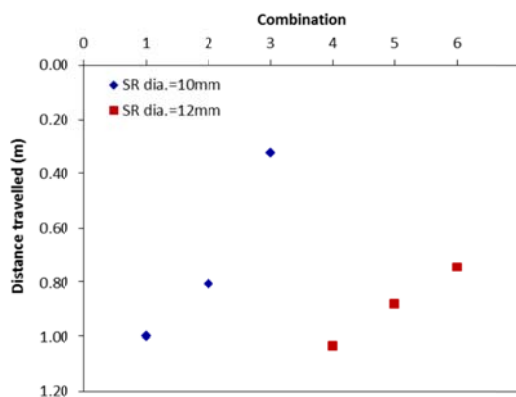


Fig. 38 Comparison of distance travelled

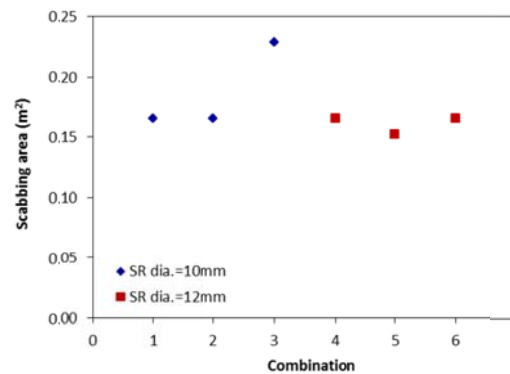


Fig. 39 Comparison of scabbing areas

## 7. Conclusions

A reliable nonlinear finite element model of reinforced concrete slabs under impact loading was developed. The structural components and their contacts were fully modeled. The erosion option of concrete and reinforcement steel was considered in the analysis. The finite element model was verified against the experiment. Three different parameter studies of the longitudinal rebar, shear bar, and concrete strengths were carried out to investigate their influence on the punching behavior of RC slabs. Different missile initial velocities of 70 m/s, 136 m/s, and 190 m/s were applied in order to consider its influence on the response of the RC slabs. The parameter studies with different combinations of reinforcement were also performed to determine the optimal design in the case of missile velocity of 136 m/s. The following conclusions have been obtained:

(1) The influence of the longitudinal rebar ratio:

In case of the missile initial velocity was 70 m/s, the longitudinal rebar ratio did not show any significant influence on punching resistance of RC slabs. In case of the missile initial velocity was 136 m/s, the longitudinal rebar ratio had a significant influence on resisting the perforation of the slabs. However, when the longitudinal rebar ratio increased from 0.45% to 1.37%, the scabbing area increased, whereas when the longitudinal rebar ratio increased from 1.37% to 3.38%, the scabbing area decreased. In case of the missile initial velocity was 190 m/s, the longitudinal rebar ratio had a significant influence on resisting the perforation of the slabs, whereas it did not show any significant influence on reducing the scabbing area.

(2) The influence of the shear rebar ratio:

In case of the missile initial velocity was 70 m/s, the shear bar ratio did not show any significant influence on punching resistance of RC slabs. In case of the missile initial velocity were 136 m/s and 190 m/s, shear bar ratio played a minimal role in resisting the perforation of the slabs, whereas it had a strong influence on reducing the scabbing area. However, when shear bar ratio increased from 0.97% to 2.48%, there was no significant effect on the scabbing resistance.

(3) The influence of concrete strength:

In case of the missile initial velocity was 70 m/s, the concrete strength did not show any significant influence on punching resistance of RC slabs. In case of the missile initial velocity were 136 m/s and 190 m/s, the concrete compressive strength did not show any significant influence on punching resistance of RC slabs, whereas the concrete tensile strength played a very important role in resisting the perforation of the RC slab. It is recommended that the concrete with high tensile strength should be used for the slab that protects against high velocity impact.

(4) For optimal design in such case of missile velocity of 136 m/s, Design-3 is recommended for resisting the perforation of the slab, while Design-5 is recommended for reducing the scabbing area.

## Acknowledgments

This work was supported by the Human Resources Development program (No. 20124030200050) of the Korea Institute of Energy Technology Evaluation and Planning (KETEP) grant funded by the Korea government Ministry of Knowledge Economy.

## References

- Daudeville, L. and Malécot, Y. (2011), "Concrete structures under impact", *Eur. J. Environ. Civil Eng.*, **15**(SI), 101-140.
- EN 1992-1-1 (2004), *Eurocode 2, Design of concrete structure - Part 1-1: General rules and rules for buildings*, Brussels.
- fib MC2010 (2013), *fib Model Code for Concrete Structures 2010*, Ernst & Sohn Publishing House, Berlin, Germany.
- Jones, N. (2012), *Structural Impact*, Second Edition, Cambridge University Press, New York, NY, USA.
- Lastunen, A., Hakola, I., Jarvinen, E., Calonius, K. and Hyvarinen, J. (2007), "Impact test facility", *Transactions of the 19th SMiRT*, Toronto, Canada, August.
- LS-DYNA (2007), *Key User's Manual*, Version 971, Livermore Software Technology Corporation, California, USA.
- Marais, S.T., Tait, R.B., Cloete, T.J. and Nurick, G.N. (2004), "Material test at high strain rate using the split Hopkinson pressure bar", *Lat. Am. J. Solid. Struct.*, **1**, 319-339.
- Martin, O., Centro, V. and Schwoertzig, T. (2012), "Finite element analysis on the Meppen-II-4 slab test", *Nucl. Eng. Des.*, **247**, 1-10.
- Martin, O., Centro, V. and Schwoertzig, T. (2012), "Finite element analysis on the VTT-IRSN flexural failure test", *Nucl. Eng. Des.*, **252**, 88-95.
- Nilson, A.H., Darwin, D. and Dolan, C.W. (2010), *Design of Concrete Structures*, Fourteenth Edition, McGraw Hill, New York, NY, USA.
- Polanco-Loria, M., Hopperstad, O.S., Børvik, T. and Berstad, T. (2008), "Numerical predictions of ballistic limits for concrete slabs using a modified version of the HJC concrete model", *Int. J. Impact Eng.*, **35**, 290-303.
- Saarenheimo, A., Tuomala, M., Calonius, K., Hakola, I., Hostikka, S. and Silde, A. (2009), "Experimental and numerical studies on projectile impacts", *J. Struct. Mech.*, **42**(1), 1-37.
- Sagals, G., Orbovic, N. and Blahoianu, A. (2011), "Sensitivity studies of reinforced concrete slabs under impact loading", *Transactions of the 21st SMiRT*, New Delhi, India, November.
- Schwer, L. (2010), *An Introduction to the Winfrith Concrete Model*, Schwer Engineering & Consulting Services, California, USA.
- Shiu, W., Donzé, F.V. and Daudeville, L. (2009), "Influence of the reinforcement on penetration and perforation of concrete targets - a discrete element analysis", *Int. J. Comput. Aid. Eng. Softw.*, **16**(1), 29-45.
- Tuomala, M., Calonius, K., Saarenheimo, A. and Välikangas, P. (2010), "Hard missile impact on prestressed shear reinforced slab", *J. Disast. Res.*, **5**(4), 437-451.
- Vepsä, A., Saarenheimo, A., Tarallo, F., Rambach, J.M. and Orbovic, N. (2011), "IRIS\_2010-Part II: Experiment data", *Transactions of the 21st SMiRT*, New Delhi, India, November.
- Zineddin, M. and Krauthammer, T. (2007), "Dynamic response and behavior of reinforced concrete slabs under impact loading", *Int. J. Impact Eng.*, **34**, 1517-1534.